Research Article

Hualei Chang, Yali Ding, Zhongqiao Zhu, Juan Zhu*

Protective effect of green synthesized nanoceria on retinal oxidative stress and inflammation in streptozotocin-induced diabetic rat

https://doi.org/10.1515/chem-2025-0189
received April 27, 2025; accepted June 13, 2025

Abstract: Oxidative stress has been identified as a significant contributing factor in developing retinal degeneration and subsequent vision loss. Hence, compounds possessing antioxidant characteristics significantly mitigate the detrimental impacts exerted on the neurological system by reactive oxygen species and free radicals. This experimental investigation assessed the neuroprotective effectiveness of rutin-mediated cerium oxide nanoparticles (R-CeO_2NPs) in a diabetic retinopathy animal model. In this study, the synthesis of R-CeO_2NPs was accomplished using rutin via a straightforward green chemistry method. The findings derived from utilizing UV–visible, X-ray diffraction (XRD), transmission electron microscopy, dynamic light scattering, and Zetasizer techniques provided evidence of the nanoscale characteristics of the biosynthesized nanoparticles. The XRD data provide evidence for the crystallization of R-CeO_2NPs in a face-centered fluorite cubic system with the Fm3m space group. Specifically, we sought to determine whether nanoceria retains its neuroprotective properties when administered after the onset of retinal degeneration. The biological evaluations showed that the synthesized R-CeO_2NPs are biocompatible and exhibited potent antioxidant activities. Animal studies revealed that the administration of the synthesized R-CeO_2NPs indicated a protective effect on retinal oxidative stress and inflammation in streptozotocin-induced diabetic rats. These findings indicate that the green synthesized CeO_2NPs can be applied as protective agent against diabetic retinopathy.

*** Corresponding author: Juan Zhu**, Department of Ophthalmology, Shaanxi Eye Hospital, Xi'an People's Hospital (Xi'an Fourth Hospital), Affiliated People's Hospital of Northwest University, Xi'an, 710004, China, e-mail: mayzhujuan@sina.com
Hualei Chang, Yali Ding, Zhongqiao Zhu: Department of Ophthalmology, Shaanxi Eye Hospital, Xi'an People's Hospital (Xi'an Fourth Hospital), Affiliated People's Hospital of Northwest University, Xi'an, 710004, China

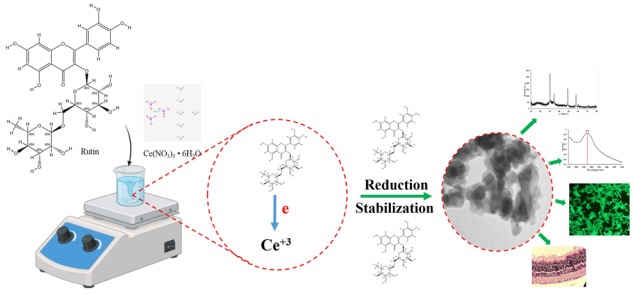

Graphical abstract

Keywords: retinal oxidative stress, inflammation, diabetic retinopathy, nanoceria

1 Introduction

Diabetes mellitus, a common chronic metabolic disease that is primarily defined by prolonged elevation of blood glucose levels and abnormal insulin secretion or function within the body, has adverse effects on different organs [1–3]. Diabetic retinopathy is one of the most devastating side effects of uncontrolled diabetes. Diabetic retinopathy is the primary etiology of acquired visual impairment in the working-age population. The development of retinopathy is influenced by abnormalities in retinal metabolism, such as heightened polyol pathway activity, augmented nonenzymatic glycation and advanced glycation end products, oxidative stress, and protein kinase C (PKC) activity [4–7]. However, the precise mechanism underlying this relationship remains unknown. Diabetes is associated with heightened oxidative stress in the retina, wherein reactive oxygen species (ROS) are believed to serve as a mechanistic connection between raised glucose levels and the metabolic irregularities that play a crucial role in the progression of diabetic problems [8–11].

In the context of diabetic retinopathy, it has been shown that inflammation may have a significant impact on both the initiation and advancement of the disease

[12]. ROS exhibit potent activation of the transcription factor nuclear factor kappa B (NF-κB), enhancing the transcriptional activity of inflammatory cytokines and chemokines, as well as enzymes involved in the manufacture of nitric oxide and prostaglandin E2. The pathophysiology of diabetic retinopathy encompasses a multitude of variables, as indicated by previous studies. Nevertheless, the precise mechanism by which oxidative stress may contribute to the pathogenesis of diabetic retinopathy has yet to be fully understood [13–16].

The inhibitory effects of antioxidants and traditional Chinese medicine on inflammatory responses have been well-established for a considerable period [17,18]. Antioxidants have been observed to exert an inhibitory effect on NF-κB activity, as well as diminish leukostasis and the production of inducible nitric oxide synthase in animal models of diabetic retinopathy [19,20]. Furthermore, it has been observed that antioxidants can impede the development of cell-free capillaries and the production of pericyte ghosts in rats with diabetes [21,22]. Furthermore, it has been observed that antioxidants can impede the generation of ROS while simultaneously enhancing the efficacy of the antioxidant defense enzyme system [23]. Hence, it is plausible that antioxidants have the potential to mitigate the physiological harm caused by oxidative stress in the retina, reduce the extent of inflammatory responses, and impede the advancement of diabetic retinopathy [24,25].

Cerium oxide nanoparticles (CeO_2NPs), also known as nanoceria (CeO_2), possess the additional benefit of exhibiting regeneration properties. Therefore, nanoceria exhibits significant promise in addressing oxidative neurological illnesses, surpassing the limitations of earlier therapeutic approaches [26,27]. This will be further elaborated upon in subsequent sections. Cerium is classified as a member of the lanthanide series, which consists of rare earth metals, according to its placement in the periodic table. The fluorite crystalline structure of cerium oxide, when coupled with oxygen in a nanoparticle (NP) formulation, exhibits distinctive antioxidant capabilities [28]. These features arise from the interplay of kinetics and thermodynamics involved in the redox processes occurring on the NP's surface. Cerium can form reversible oxygen bonds and transition between Ce^{4+} and Ce^{3+} oxidation states in response to oxidizing and reducing circumstances. The occurrence of oxygen vacancies in the NP lattice is concomitant with the depletion of oxygen and the conversion of Ce^{4+} to Ce^{3+}. Nanoceria has been shown to exhibit both superoxide dismutase (SOD) and catalase (CAT)-like activity. This dual capability grants nanoceria the capacity to replenish its antioxidant activity. The proposed paradigm entails the utilization of Ce^{3+} nanoceria to catalyze the reduction of O^{2-} species, resulting in the formation of hydrogen peroxide (H_2O_2) and the oxidation of Ce^{3+} to Ce^{4+}. The H_2O_2 that is produced can then undergo a reaction with cerium ion (Ce^{4+}) to restore the cerium ion to its trivalent state (Ce^{3+}) and generate molecular oxygen. Given these facts, we applied the green chemistry method to synthesize CeO_2NPs to alleviate the oxalate stress induced by diabetic conditions on the retina. It is the first report on rutin-assisted CeO_2NPs (R-CeO_2NPs) and their application as a retinoprotective agent. The most important significance and novelty of this research resides in applying the green synthesis method using rutin as the reducing and stabilizing agent to obtain sophisticated CeO_2NPs with potent antioxidant activities, where no studies were found with rutin for the synthesis of CeO_2NPs. Moreover, the application of the R-CeO_2NPs for treating diabetic retinopathy is novel.

2 Materials and methods

2.1 Materials

Materials used were $Ce(NO_3)_3{\cdot}6H_2O$ (Merck, Germany), rutin (Sigma-Aldrich, USA), Dulbecco's Modified Eagle Medium (DMEM; Gibco, Canada), phosphate buffered saline (Gibco, Canada), pen/strep (Gibco, Canada), fetal bovine serum (FBS; Gibco, Canada), and dimethyl sulfoxide (Sigma-Aldrich, USA). All chemicals utilized in the experiment were of analytical grade and had been previously employed, except for those subjected to additional purification. The experiment employs ultrapure grade water.

2.2 Synthesis of R-CeO_2NPs

According to the previous reports, the present investigation involved the synthesis of CeO_2(IV)NPs using a sol–gel technique [29,30]. The cerium precursor employed in this process was $Ce(NO_3)_3{\cdot}6H_2O$, while rutin was utilized as the reducing and stabilizing agent, and distilled water served as the solvent (Schematic 1). In order to carry out the synthesis, a mass of 4.37 g of cerium nitrate was dissolved in 50 mL of distilled water in a 200 mL round bottom flask. The resulting mixture was stirred (~400 rpm) at room temperature for 20 min. Subsequently, the cerium nitrate solution was cautiously introduced into 30 mL of rutin (100 mM) [31], and the resulting mixture was then put into a container for further placement in an oil bath. The

combination solution was subjected to stirring at a temperature of 80°C for 24 h in order to obtain a gel-like substance. After the completion of the route, the gel obtained was subjected to a drying process at a temperature of 110°C for 6 h. In order to complete the procedure, the gels that were formed were subjected to calcination at a temperature of 400°C for 2 h. This step led to the successful synthesis of yellow-colored CeO_2NPs.

2.3 Characterization of R-CeO_2NPs

The synthesized R-CeO_2NPs were characterized using various experimental techniques to reveal the physicochemical properties [32,33]. UV–vis spectroscopy was conducted to determine the absorbance band of R-CeO2NPs in DI water within the 200–800 nm wavelength range. To conduct dynamic light scattering (DLS) analysis, a solution of R-CeO_2NPs was prepared by dissolving them in deionized water at a ratio of 1:100. The solution was then subjected to sonication and subsequently examined at a temperature of 25°C using the Malvern Zetasizer. X-ray diffraction (XRD) examination was conducted on R-CeO_2NPs generated through phytosynthesis. The XRD analysis employed CuKα radiation with a wavelength (λ) of 1.54060 Å and a Ni monochromator was utilized. The analysis was completed within a 2θ range from 10° to 80°. The morphology of the manufactured R-CeO_2NPs was examined using transmission electron microscopy (TEM) and scanning electron microscopy (SEM) analysis. The samples were prepared under ambient conditions in order to conduct SEM and TEM analysis. This was achieved by applying the R-CeO_2NPs in methanol (1 mg/mL) over copper grids previously coated with a layer of carbon using a drop-wise coating method. The surplus NP solution was eliminated using filter paper. The copper grid was subsequently dried at room temperature and subjected to TEM investigation using the Tecnai F20 model instrument, which runs at an accelerating voltage of 200 kV.

2.4 *In vitro* evaluations

2.4.1 Antioxidant potential of R-CeO_2NPs

2.4.1.1 Antioxidant 2,2-diphenyl-1-picrylhydrazyl (DPPH) assay

The antioxidant capacity of R-CeO_2NPs was assessed using a methodology previously established by other researchers [34,35]. The antioxidant capacity of various concentrations of R-CeO_2NPs (10, 25, 50, and 100 µg/mL) was examined. The reaction mixture consisted of 1 mL of DPPH and 1 mL of R-CeO_2NPs at varying concentrations. The solution was rapidly agitated and incubated at ambient temperature for 30 min. Subsequently, the optical density was determined at a wavelength of 517 nm.

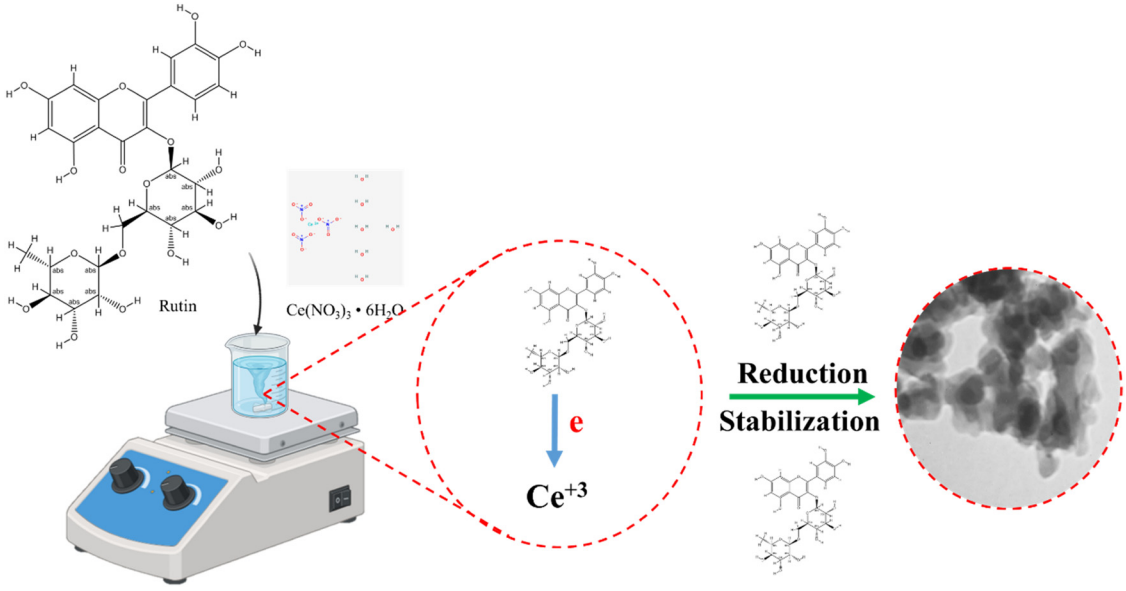

Schematic 1: Illustration of the synthesis of CeO_2NPs using rutin.

2.4.1.2 H_2O_2 antioxidant assay

The method proposed by Yakoob et al. [36] was employed to evaluate the H_2O_2 assay. The reaction mixture consisted of different doses of R-CeO_2NPs (10, 25, 50, and 100 µg/mL), 300 µL of phosphate buffer (50 mM, pH 7.4), and 600 µL of H_2O_2 (2 mM H_2O_2 in phosphate buffer, 50 mM, pH 7.4). The combination underwent vigorous shaking for 10 min, following which the absorbance was quantified at a wavelength of 230 nm using a spectrophotometer (Model U-2900).

2.4.2 Cellular cytotoxicity of R-CeO_2NPs

The cytocompatibility of R-CeO_2NPs was investigated using a cell line of corneal epithelial cells known as SIRC. Various concentrations of R-CeO_2NPs (10, 25, 50, and 100 µg/mL) were examined to assess their acute and chronic toxicities. The cells were cultured in DMEM supplemented with 10% FBS. They were then plated in 96-well plates at a density of 3.5×10^5 cells per well and incubated at 37°C in a carbon dioxide (CO_2) incubator with 5% CO_2 for 24 h before introducing NPs. Following the introduction of NPs, the plates were subjected to an additional 24 h incubation period before conducting the MTT experiment. The absorbance at 560 nm was measured using the MTT test, with a background absorbance recorded at 690 nm. Positive controls consisted of untreated cells exhibiting 100% vitality, while blanks comprised cells without the inclusion of assay reagents.

2.5 Animal studies to assess efficacy of R-CeO_2NPs in a diabetic retinopathy rat mode

2.5.1 Experimental design and model induction

Based on prior research, the model was induced by applying streptozotocin (STZ), with a minor adjustment in administration timing and dosage of STZ [37]. The Zhinanzhen Biology Ethics Committee approved the studies conducted on animals in our research organization(s), No.: A2025000119. Before approval, these entities ensured that the experiments conformed to all essential guidelines, regulations, and legal and ethical standards pertaining to animal research. All experimental procedures complied with the Animal Research: Following the Vivo Experiments (ARRIVE) guidelines. The animal enclosure was maintained at a consistent temperature of 23°C, accompanied by sufficient air circulation. Throughout the trial, the animals were provided unhindered access to standard feed and water. Except for the control group, all groups of rats were administered a solitary intraperitoneal (i.p.) injection of 60 mg/kg STZ, which was dissolved in a 0.05 mol/L citrate buffer (pH 4.5) and administered within 10 min. The task was completed within 2 days. Blood glucose levels were utilized to identify instances of hyperglycemia in animals. This study exclusively included animals whose blood glucose levels were above 300 mg/dL. The animals were allocated into three groups using a random process: the healthy group (consisting of animals that did not undergo any induction or therapy), the negative control group (comprising diabetic animals that did not receive any treatment), and the treated group (comprising diabetic animals that were treated with R-CeO_2NPs (85 mg/kg) via the i.p. injection).

2.5.2 Antioxidant capacity evaluation

After passing the treatment time point, the retinal tissues were harvested and homogenized in ice-culled sodium phosphate buffer. The obtained tissues were centrifuged at 1,000*g* for 20 min at 4°C, and the resultant supernatant was collected and applied for antioxidant capacity measurement. The antioxidant capacity was evaluated by measuring lipid peroxidation, glutathione peroxidase (GPx), CAT, and SOD. The measurements were conducted using specific commercial kits (Sigma-Aldrich, St Louis, MO) following the manufacturer's protocol.

2.5.3 Real-time PCR

The changes in the expression pattern of the target genes (heme oxygenase-1 [HO-1] and nuclear factor erythroid 2-related factor 2 [Nrf2]) were evaluated using the RT-PCR. The total RNA was isolated and applied to synthesize cDNA using SYBR Green and Reverse Transcriptase. A thermocycler was used to amplify according to the manufacturer's protocol. GAPDH was used as a reference gene, and the expression level was determined using the $2^{-\Delta\Delta Ct}$ method.

2.5.4 Histological analysis

Following the period of isolation, the retinas of the rats were immersed in a solution containing 4% paraformaldehyde. Following that, retinal tissues were sliced into 5 µm sections, which were then subjected to staining with E&H.

Subsequently, the sections were observed using an operational microscope. The high-resolution digital camera system (C3040-AD6, Shanghai, China) was utilized to collect the photographs. This system was connected to both the operational microscope and the desktop computer. Retinal images were captured at a consistent distance of 1,500 mm from the optic nerve in both eyes.

2.6 Statistical analysis

The quantitative results were presented as mean value ± standard deviation. The statistical analysis was conducted using appropriate methods, such as Student's *t*-test, one-way ANOVA, or two-way ANOVA, depending on the specific requirements of the study. The normality of the data was verified using the Kolmogorov–Smirnov test. Statistical significance was attributed to all values of $p < 0.05$, whereas values of $p > 0.05$ were deemed statistically inconsequential.

3 Results and discussion

3.1 Physicochemical properties of R-CeO_2NPs

The confirmation of R-CeO_2NPs generation from rutin was initially verified using UV–vis absorption spectroscopy in the wavelength range of 150–500 nm. UV–vis spectroscopy is widely recognized as a crucial technique for characterizing NPs and determining their optical characteristics. Figure 1 presents the UV–vis absorption spectra of the R-CeO_2NPs generated using biological means. The R-CeO_2NPs exhibited a maximum absorption peak at around 275 nm, which can be attributed to the charge transfer transition from O2P to Ce4f [38]. Maqbool et al. [39] have documented comparable UV–vis spectra for CeO_2NPs produced using extracts derived from *Olea europaea* leaves. Furthermore, the optical band gap of the CeO_2NPs was determined to be 4.5 eV based on the analysis of the UV–visible spectral data using the Tauc equation [40].

To validate the synthesis and assess the biological activity of R-CeO_2NPs, it is imperative to evaluate key parameters such as the average particle size, radius, crystalline characteristics, and surface charge of R-CeO_2NPs. The SEM and TEM pictures provided visual evidence that the average particle size of R-CeO_2NPs was measured to be

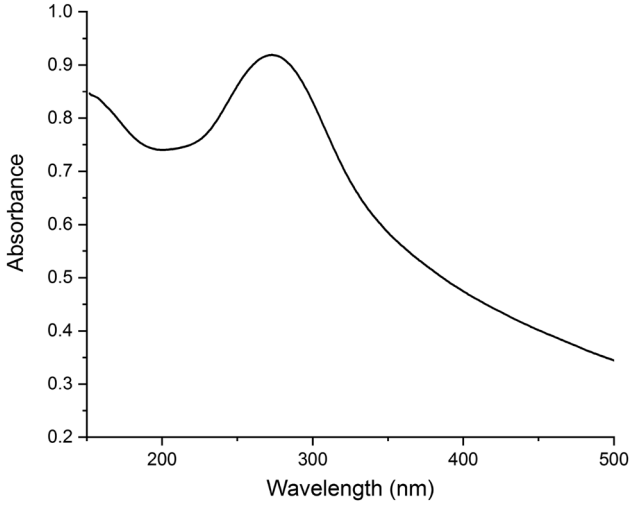

Figure 1: UV–vis spectrum of R-CeO_2NPs in the solution stat (DI water) with a maximum absorption peak at about 275 nm.

85.0 ± 25.1 nm (Figure 2). The SEM/TEM images showed that the synthesized R-CeO_2NPs have a spherical morphology with uniform size. A narrow distribution indicates a slight variance in the particle diameters of uniformly sized NPs, which are all the same size or almost the same. This is frequently a desired feature for many applications because it can result in more consistent and predictable qualities. According to a study on the size dependency of gold NPs, uniform NPs have consistent characteristics like surface area and density, making them more effective in applications like drug administration or catalysis [41]. Uniformity guarantees consistent performance since a NP's size might directly impact its function in certain situations.

The utilization of DLS in the present investigation is justified due to its ease of operation and ability to decrease the interference caused by multiple light scattering from suspended particles. Particles are spread throughout the liquid medium, specifically water-based solutions, and these particles' average size distributions are considered hydrodynamic diameters [42]. In a broad sense, the presence of dispersed particles leads to the formation of interfaces due to the processes of dissolution and adsorption involving co-ions (ions with the same charge) or counter ions (ions with opposite charge). Interacting forces within the dispersed medium in DLS result in a diverse range of particle aggregation. The primary factor leading to the lack of a strong correlation between the hydrodynamic diameter measured by DLS and other size determination techniques, such as SEM and TEM, is agglomerates forming from inevitable interfacial interactions [43,44]. Figure 3a represents the DLS result of the synthesized R-CeO_2NPs.

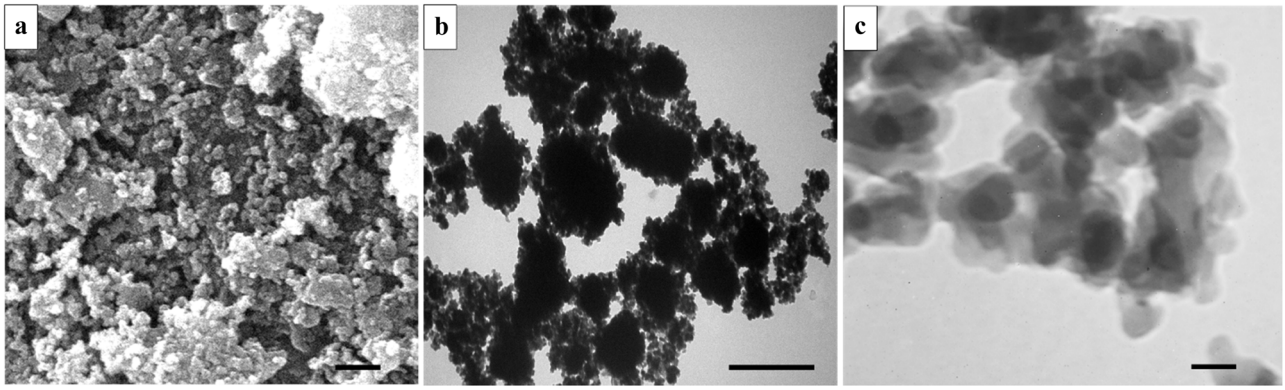

Figure 2: (a) SEM (scale bar: 400 nm), (b) TEM (scale bar: 500 nm), and (c) TEM (scale bar: 100 nm) images of the R-CeO_2NPs synthesized using rutin solution. The images showed that the R-CeO_2NPs have a spherical morphology with uniform shape.

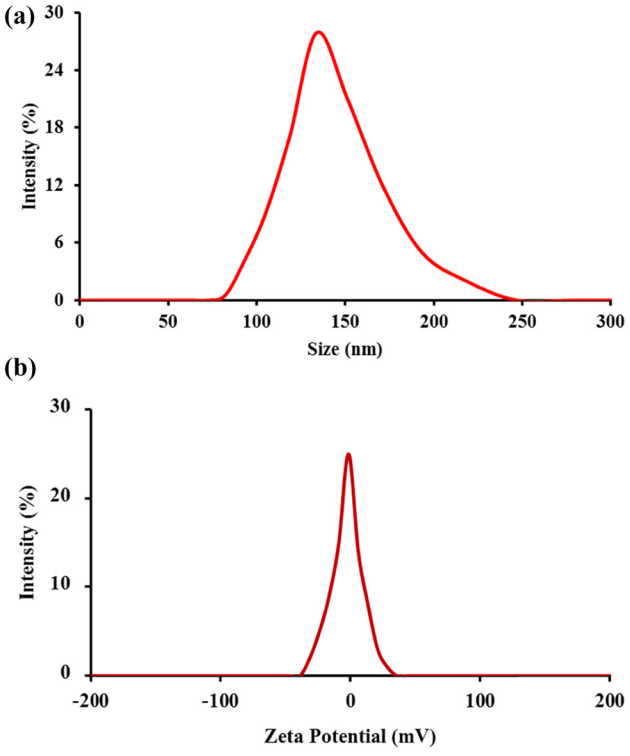

Figure 3: (a) DLS and (b) zeta potential of R-CeO_2NPs in DI water (0.1 mg/mL synthesized using rutin solution. Results showed hydrodynamic diameter of 154.3 ± 19.4 nm with the polydispersity index of 0.21 and zeta potential of 12.3 ± 2.4 eV.

The application of an electric field to colloidal particles induces electrokinetic phenomena. The aforementioned effects typically have significant implications for the electrical charges present on the surface of colloidal particles. The term "zeta potentials" refer to the magnitude of the net surface charge. Various elements, including the velocity of the moving particle in response to an electric field and the viscosity of the dispersion medium, influence the zeta potentials. Compared to bigger particles, smaller particles exhibit more mobility and velocity inside a less viscous medium, resulting in enhanced diffusion rates and increased stability [45]. Zeta potential measurements are conducted to assess the stability of particles in a colloidal dispersion. The zeta potential magnitude indicates the level of electrostatic repulsion between co-ions inside a colloidal dispersion [42,46,47]. Particles with high zeta potential values indicate enhanced stability and reduced susceptibility to agglomeration.

Nevertheless, particles occasionally demonstrate a zero surface charge, often assessed at a specific pH level. The absence of surface charge is commonly referred to as the isoelectric point (IEP) or the point of zero charge. Several studies have documented varying (IEP pH values for CeO_2 in a particular electrolyte solution. Gulicovski et al. [48] observed two distinct pHiep values, pHiep 7.6 and pHiep 6.7, when employing KNO_3 as the electrolyte. The authors emphasized that the observed change in pHiep values, namely from pHiep 7.6 to pHiep 6.7, can be related to the adsorption of SO_4^{2-} ions. This suggests that the dispersion's excess co-ions or counter-ions influence the shift. This phenomenon could perhaps account for the variations in reported pHiep values for CeO_2 observed across multiple literature sources within a certain electrolyte environment.

The XRD method was employed to validate the crystalline characteristics of the NPs. Figure 4 displays the powder XRD patterns of the R-CeO_2NPs produced using a rutin solution. The XRD pattern revealed the presence of many crystallographic planes, namely (111), (200), (220), (311), and (222), which are associated with the CeO_2 material. The patterns were compared to the JCPDS file 01-075-0390, and it was observed that cubic CeO_2 exhibited

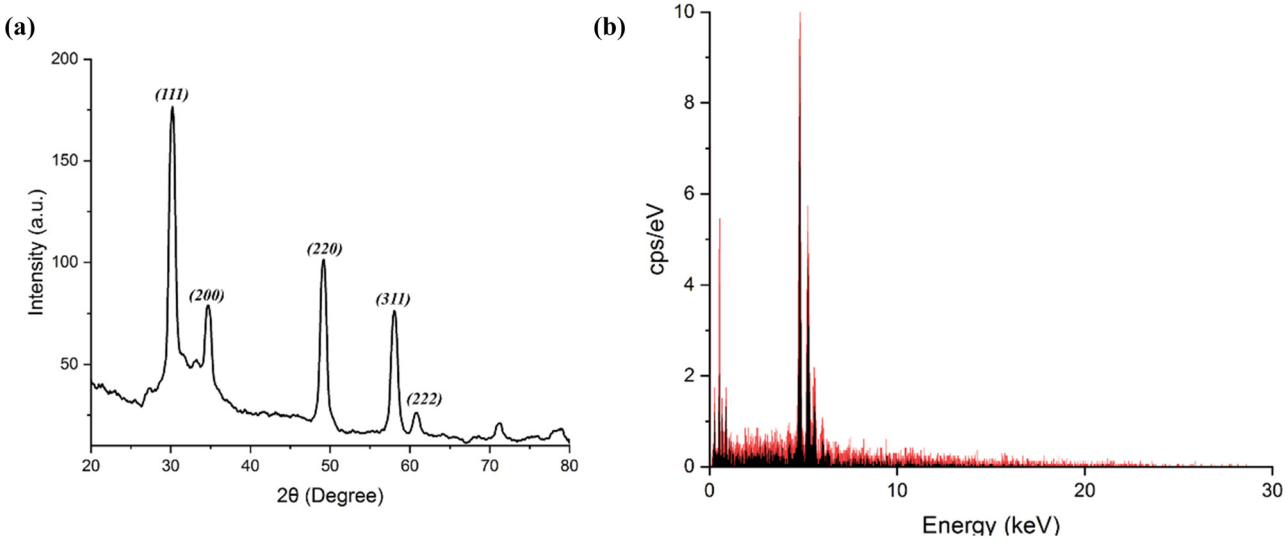

Figure 4: (a) XRD pattern and (b) EDX spectrum of the R-CeO_2NPs synthesized using rutin solution. The XRD pattern revealed the presence of many crystallographic planes, namely (111), (200), (220), (311), and (222). The EDX analysis (b) showed that the synthesized R-CeO_2NPs were mainly composed of Ce (79.2%) and O (20.8%).

identical peaks and planes that matched with the reference file. The XRD data provide evidence for the crystallization of R-CeO_2NPs in a face-centered fluorite cubic system with the Fm3m space group, which aligns with the standard JCPDS card no. 34-0394 [49,50]. After calcination, it was noted that no further distinctive peaks were present in the pattern, suggesting that the biosynthesized R-CeO_2NPs are of high purity. The energy dispersive X-ray (EDX) analysis (Figure 4b) showed that the synthesized R-CeO_2NPs were mainly composed of Ce (79.2%) and O (20.8%).

The surface functional groups of the components (pure rutin and R-CeO_2NPs synthesized using rutin solution) were evaluated using FTIR spectroscopy. The results (Figure 5) showed that the characteristic peaks of rutin are presented in the R-CeO_2NPs synthesized using rutin solution. The R-CeO_2NPs exhibit a wide peak around 3,380 cm^{-1} that can be related to the O–H stretching vibrations of phenols. The peaks around 1,120, 1,640, and 2,891 cm^{-1} can be related to C═O, –C═C–, and C–H of –COOH group, respectively. These findings confirmed that the synthesized R-CeO_2NPs are

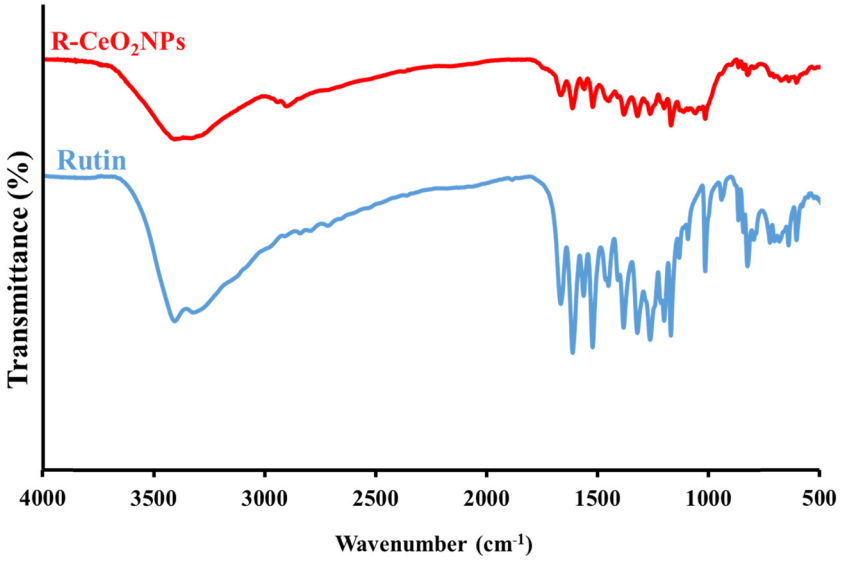

Figure 5: FTIR spectra of rutin and R-CeO_2NPs synthesized using rutin solution. The peaks around 1,120, 1,640, and 2,891 cm^{-1} can be related to C═O, –C═C–, and C–H of –COOH group, respectively.

Table 1: Physicochemical properties of R-CeO_2NPs

Actual size	Diameter (nm)	Polydispersity index	Zeta potential (mV)	UV–vis λ_{max} (nm)	Crystallographic planes
85.0 ± 25.1	154.3 ± 19.4	0.21	12.3 ± 2.4	257	(111), (200), (220), (311), and (222),

decorated with rutin polyphenolic compounds responsible for reducing salt and capping the NPs. Table 1 summarizes the physicochemical properties of R-CeO_2NPs.

3.2 Biological activities of R-CeO_2NPs

3.2.1 Antioxidant activities

The DPPH antioxidant assay was employed to evaluate the antioxidant potential of R-CeO_2NPs generated by a green synthesis method in combating free radicals. The disruption of physiological processes and mutations in macromolecules, including DNA, RNA, proteins, and lipids, can be attributed to the imbalance between the creation of ROS and their quenching by the endogenous antioxidant system. Additionally, this imbalance can accelerate cellular stress in cell signaling pathways. The presence of a high concentration of glucose can expedite the production of ROS through multiple mechanisms. These mechanisms include glucose auto-oxidation, oxidative phosphorylation, activation of PKC C, glycation (the non-enzymatic bonding of free reduced sugar with free amino acids such as DNA and RNA), hexosamine metabolism, and methylglyoxal formation [51–53]. The results (Figure 6a) showed that the synthesized R-CeO_2NPs exhibited potent and dose-dependent DPPH radical-neutralizing activity. While these assays can provide valuable information, they do not

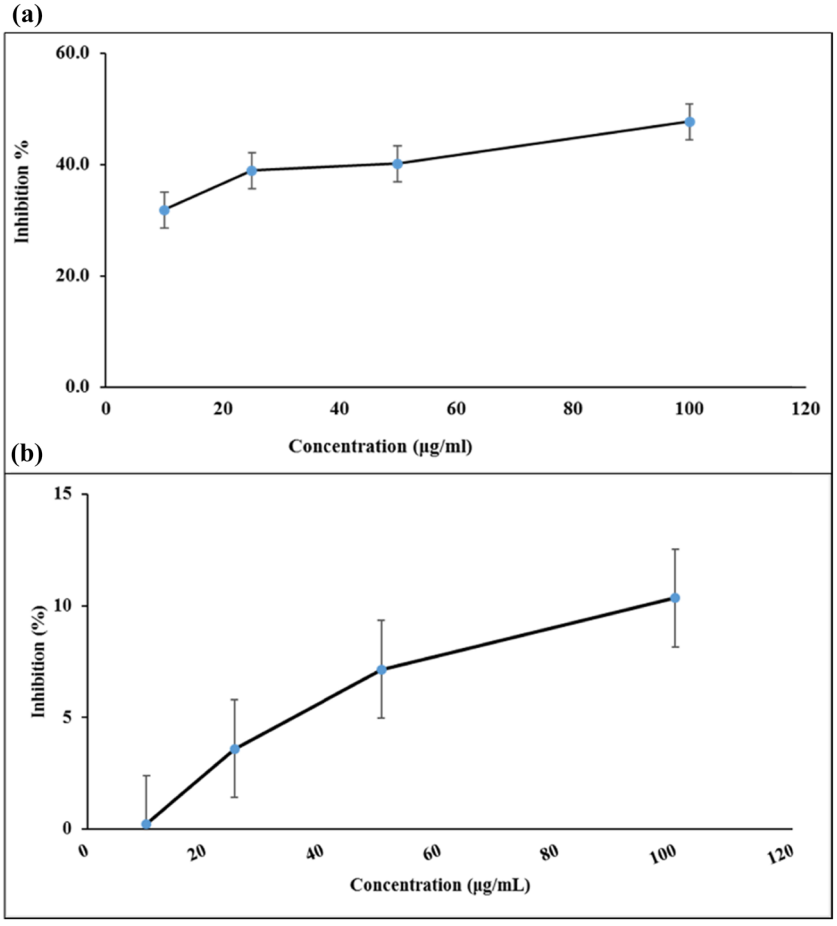

Figure 6: Antioxidant activities of R-CeO_2NPs: (a) DPPH radical inhibition percentage and (b) H_2O_2 radical inhibition percentage. The results showed dose-dependent radical scavenging activities against DPPH and H_2O_2 free radical, with the highest antioxidant activities at 100 µg/mL.

perfectly replicate the complex and dynamic *in vivo* environment. *In vivo*, oxidative stress is influenced by various factors, including hyperglycemia, hypoxia, inflammation, and the presence of other reactive species.

H_2O_2 induces the production of hydroxyl radicals, which then initiate lipid peroxidation within susceptible cells, leading to DNA damage and subsequent cellular demise. Acute exposure to H_2O_2 can jeopardize the health of an individual. H_2O_2 induces skin irritation upon direct touch. Mitochondria are cellular organelles that are synthesized through the action of a specific enzyme, which plays a crucial role in regulating cellular processes related to growth and programmed cell death. Nevertheless, the cellular environment already contains the enzyme responsible for the decomposition of H_2O_2 prior to its conversion into hydroxyl radicals [54]. The synthesis of H_2O_2 within cellular structures serves as a mechanism to safeguard the body against highly hazardous substances such as superoxide radicals. However, in instances where an organism experiences pathological conditions, the activity of these enzymes diminishes, resulting in an elevation of H_2O_2 levels beyond their normal thresholds. Consequently, the capacity to eliminate H_2O_2 and prevent lipid peroxidation is compromised [55]. The present investigation has revealed that using R-CeO_2NPs exhibits notable and dose-dependent efficacy in reducing cellular H_2O_2 levels (Figure 6b).

3.3 Cellular cytotoxicity

The possible cellular toxicity of the synthesized R-CeO_2NPs was evaluated using the MTT assay method. The results (Figure 7) showed that the synthesized R-CeO_2NPs did not induce significant toxic effects.

We also applied the live/dead staining to visualize and confirm the results of the MTT assay, which are presented in Figure 8. Although the MTT assay and live/dead staining are techniques used to evaluate cell viability, their concepts and uses differ. While live/dead staining employs fluorescent dyes to distinguish between live and dead cells visually, MTT tests are colorimetric and measure the metabolic activity of living cells. Direct counting of living and dead cells is made possible by live/dead staining, which visually depicts cell viability. The results showed that the treatment using R-CeO_2NPs did not induce cell death.

3.4 Animal studies result

Animal studies on STZ-induced diabetes were conducted to evaluate the efficacy of the proposed therapy. First, we evaluated the effect of STZ administration and R-CeO_2NPs on food ingestion, insulin level, and HbAc1 level, and the results are presented in Figure 9 and Table 2. We found that the diabetic induction using STZ significantly increased the daily food ingestion ($p < 0.05$), while the treatment using R-CeO_2NPs modulated the daily food ingestion. We measured the serum insulin level and found that the diabetic induction using STZ significantly decreased the serum insulin level ($p < 0.05$), while treatment using R-CeO_2NPs slightly increased the serum insulin level. We also measured the HbA1c level and found it was significantly high in STZ-induced diabetic rats. The treatment using R-CeO_2NPs

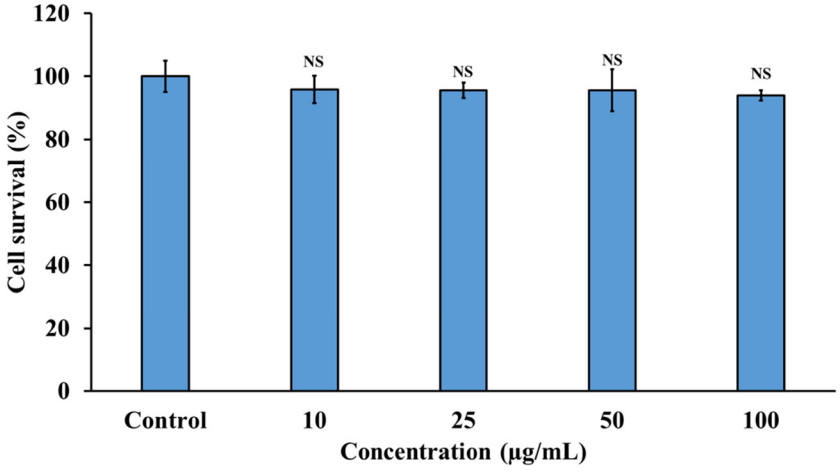

Figure 7: Cellular cytotoxicity of R-CeO_2NPs against corneal epithelial cells. All values are expressed as mean ± SD ($n = 3$). (NS, not significant. Analyzed using one-way ANOVA followed by Tukey's test as a *post hoc* analysis. The results showed that the R-CeO_2NPs did not induce significant toxicity at each concentration.

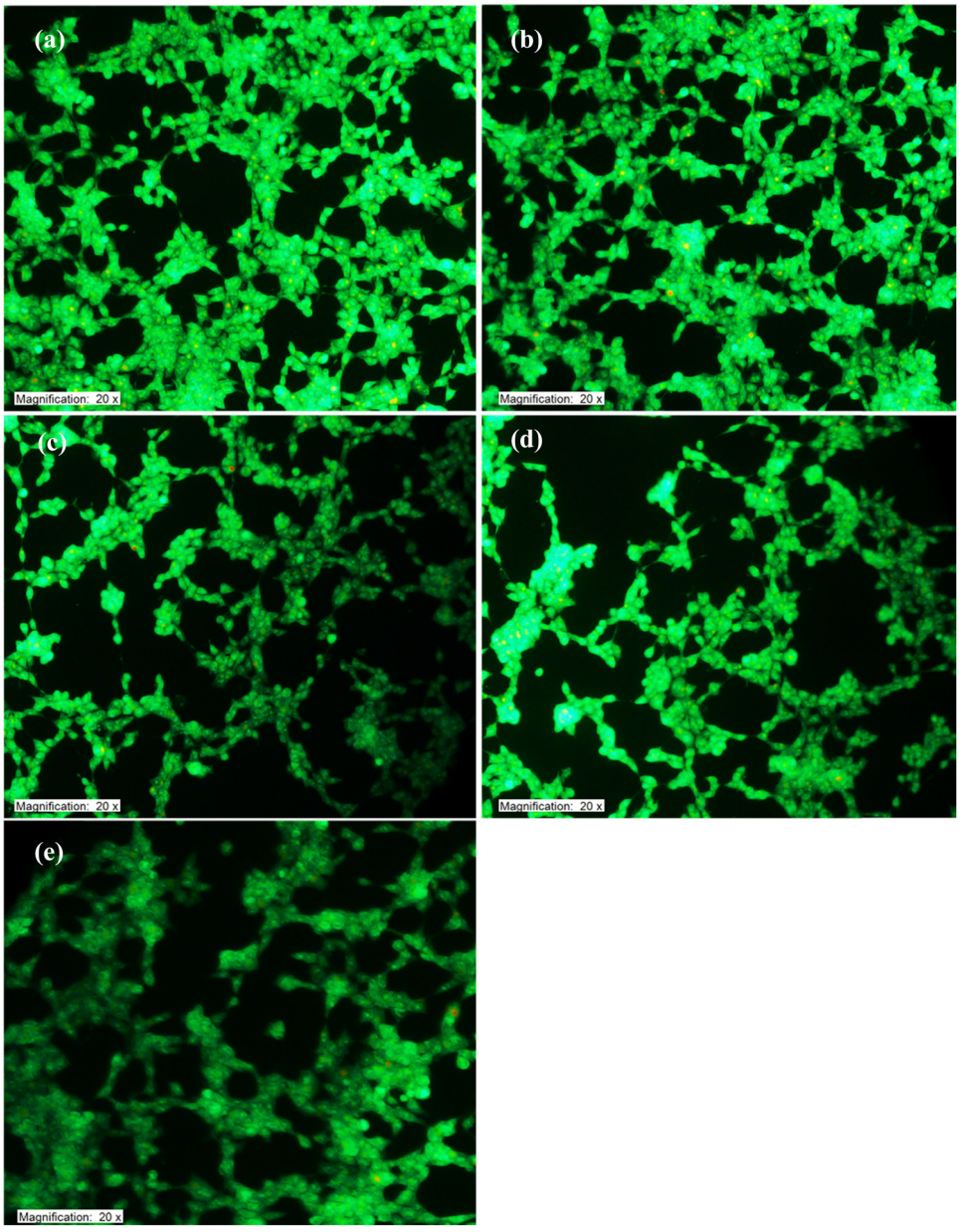

Figure 8: Live/dead assay of the cells under treatment with (a) 0 μg/mL, (b) 10 μg/mL, (c) 25 μg/mL, (d) 50 μg/mL, and (e) 100 μg/mL of R-CeO_2NPs. The results showed that the R-CeO_2NPs did not induce significant toxicity at each concentration.

slightly decreased the HbA1c level, but it was significantly higher than in the healthy animals. It has been demonstrated that CeO_2NPs increase insulin sensitivity in skeletal muscle and adipose tissue, possibly through improving mitochondrial activity [56]. By scavenging free radicals and lowering the generation of ROS, CeO_2NPs can help reduce oxidative stress, which is a major contributing factor to the development of insulin resistance. Although CeO_2NPs have not been shown to lower HbA1c directly, their ability to increase insulin sensitivity and lessen oxidative stress may indirectly do so. Blood sugar levels can be controlled by lowering oxidative stress and increasing insulin sensitivity. HbA1c is a measurement of average blood glucose levels over several months. One of the main contributing factors to the pathophysiology of type 2 diabetes is oxidative damage, which CeONPs can alleviate the oxidative stress and shield beta cells from damages [57].

This study aims to investigate the retinal microstructure and potential ultrastructural alterations that occur during hyperglycemia and subsequent therapy. Upon histological examination using hematoxylin and eosin staining, it was observed that the retinas of typical rats

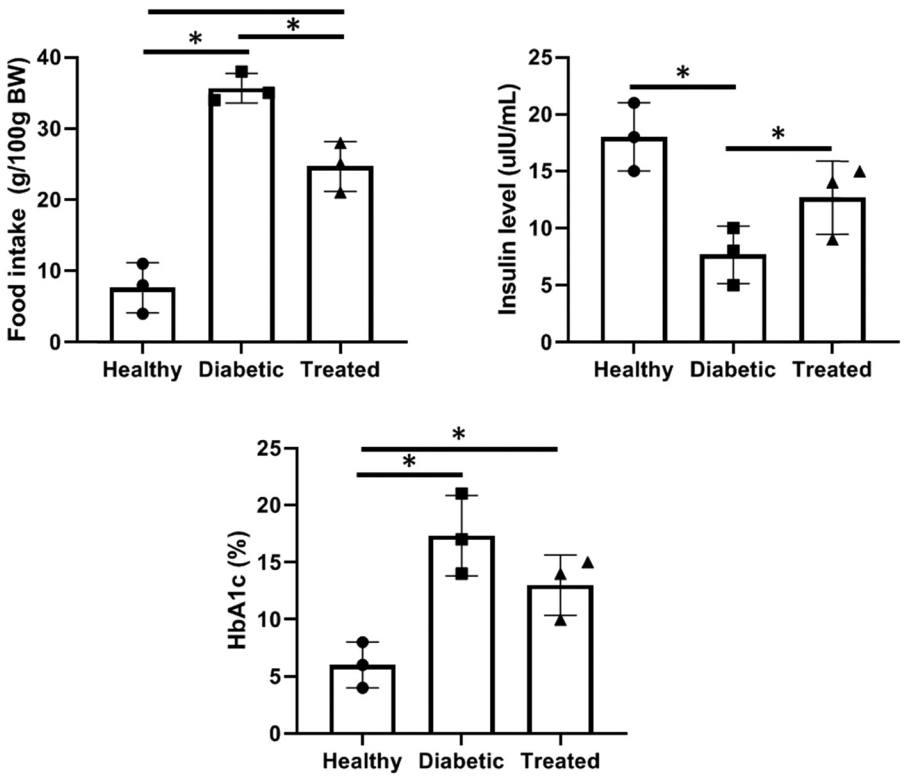

Figure 9: Effects of R-CeO_2NPs on food intake, serum insulin, and glycated hemoglobin (HbA1c) on STZ-induced diabetic rats. All values are expressed as mean ± SD (n = 5). (*) $p < 0.05$. (**) $p < 0.01$. Analyzed using one-way ANOVA followed by Tukey's test as a *post hoc* analysis.

Table 2: Effects of R-CeO_2NPs on food intake, serum insulin, and glycated hemoglobin (HbA1c) on STZ-induced diabetic rats and HbA1c level

	Healthy	Diabetic	Treated
Food intake (g/100 g BW)	7.66 ± 3.51	35.66 ± 2.8	24.65 ± 3.51
Insulin level (uIU/mL)	18.0 ± 3.1	7.66 ± 2.51	12.66 ± 3.21
HbA1c (%)	6.03 ± 1.85	17.33 ± 3.50	13.0 ± 2.64

exhibited a smooth appearance. The cellular distribution throughout each stratum exhibited a consistent pattern and well-organized structure, as depicted in Figure 10 (Healthy). The observed structure was characterized by its clarity and completeness. The retinal cells within the group of rats with diabetes exhibited signs of disorganization, swelling in the nerve fiber layer, and an observed increase in capillaries (Figure 6b). The degenerative

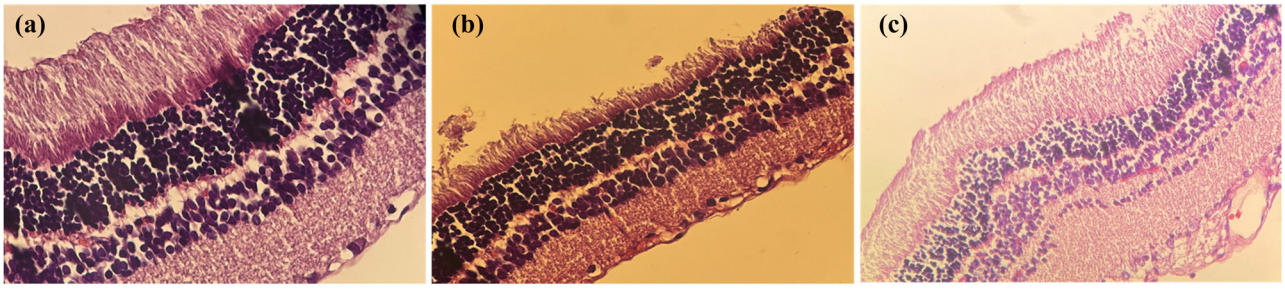

Figure 10: Effects of R-CeO_2NPs on histopathological changes in the diabetic rat retinas: (a) healthy animal, (b) negative control (diabetic animals without treatment), and (c) treatment (diabetic animals treated with R-CeO_2NPs). Results showed that the treatment using R-CeO_2NPs alleviated the thinning of retina induced by the diabetic condition.

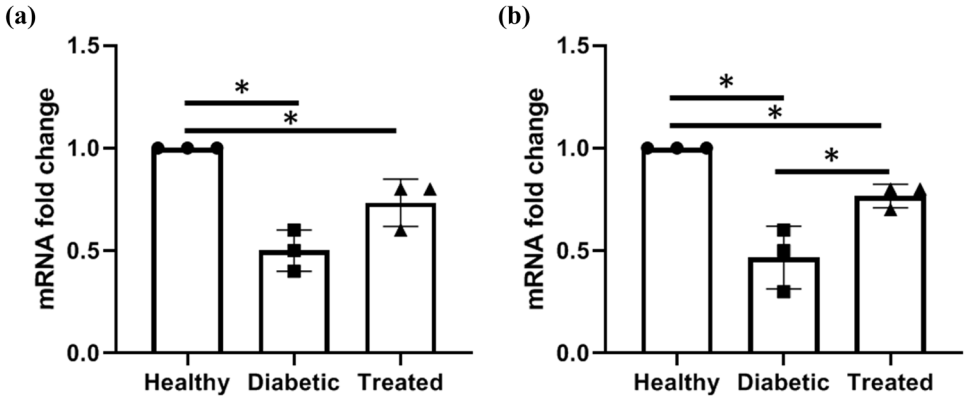

Figure 11: mRNA expression level of (a) Nrf2 and (b) HO-1 under treatment with R-CeO_2NP. All values are expressed as mean ± SD (n = 5). (*) $p < 0.05$. Analyzed using one-way ANOVA followed by Tukey's test as a *post hoc* analysis. The results showed that the treatment using R-CeO_2NPs modulated the expression of Nrf2 and HO-1 mRNA.

changes induced by diabetes were effectively corrected with the therapy of produced R-CeO_2NPs mediated by rutin, as demonstrated in Figure 10 (Treated). The measurement and statistical analysis of retinal thickness were conducted. The retinal thickness in the diabetic group was observed to be improved by the R-CeO_2NPs generated by rutin mediation. However, it is important to note that this impact did not reach statistical significance.

The effects of R-CeO_2NPs on gene expression level were evaluated using the PCR technique, and the results are

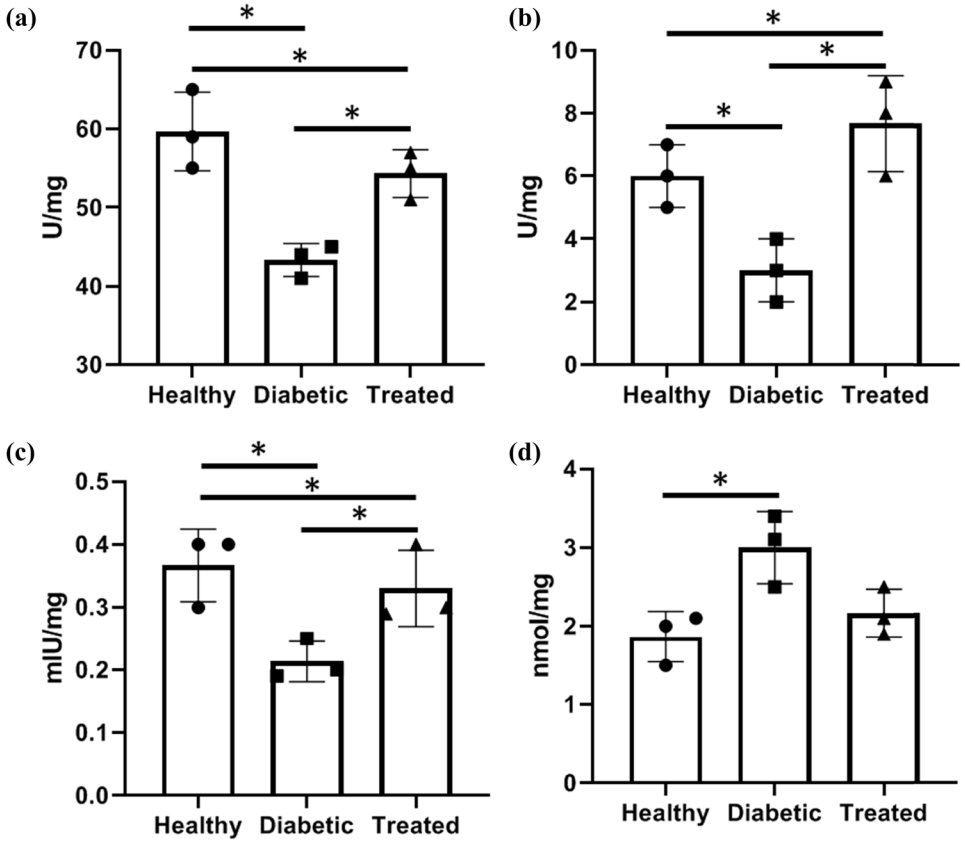

Figure 12: Oxidative state of the tissue under treatment with R-CeO_2NPs. (a) SOD, (b) CAT, (c) GPx, and (d) malondialdehyde. All values are expressed as mean ± SD (n = 5). (*) $p < 0.05$. Analyzed using one-way ANOVA followed by Tukey's test as a *post hoc* analysis. The results showed that the treatment using R-CeO_2NPs enhanced antioxidant content and reduced the oxidative stress state.

presented in Figure 11. We found that the diabetic induction using STZ significantly suppressed the expression of Nrf2 mRNA levels. On the other hand, the treatment using R-CeO_2NPs recovered the suppressed effect and improved the expression of Nrf2 mRNA (Figure 11a). It has been established that Nrf2 shields cells against both internal and external stressors. In addition to playing a significant function as a negative regulator of inflammation, which attenuates inflammation-associated pathogenesis in various disease situations, Nrf2 is thought to be a component of the most significant cellular system that protects against oxidative stress. Nrf2 has been linked to significant protective effects, particularly in disease processes with prominent inflammation and ROS. Essentially, Nrf2/HO-1 signaling can be activated by antioxidant NPs, which can set off a series of events that improve the cell's resistance to oxidative stress and potential harm. It was hypothesized that R-CeO_2NPs protect against retina tissue damage by activating Nrf2/HO-1 signaling by increasing the levels of Nrf2 and Bcl-2 and endogenous antioxidants like HO-1, glutathione peroxidase (GSH), and SOD.

We also evaluated the mRNA expression level of HO-1 and found that STZ significantly suppressed the expression level, and the treatment using R-CeO_2NPs recovered the suppressive effect (Figure 11b). Accordingly, it can be concluded that the treatment using R-CeO_2NPs recovered attenuated the diabetic oxidative stress.

The onset and advancement of diabetic retinopathy are significantly influenced by oxidative stress. By harming cells and tissues, oxidative stress causes inflammation as well as changes in structure and function, which in turn causes retinal damage. Oxidative stress in the retina is caused by metabolic irregularities brought on by high blood glucose levels in diabetes, which also lower antioxidant defenses and increases the production of ROS. Oxidative stress can harm blood vessels and retinal cells, resulting in lipid peroxidation, inflammation, apoptosis (programmed cell death), and structural and functional alterations. Although more clinical trials are required to validate these results, research indicates that antioxidant therapy may help manage diabetic retinopathy by increasing antioxidant defenses and reducing ROS generation [58,59]. We measured SOD, CAT, GPx, and malondialdehyde to evaluate the oxidative state of the tissue under treatment with R-CeO_2NPs, and found that the treatment using R-CeO_2NPs alleviated the oxidative stress of the tissue (Figure 12).

Several studies have shown promising potential of antioxidant NPs as retinoprotective against diabetic retinopathy, and this study's results align with those reports. Li et al. [60] synthesized a ROS-responsive drug delivery system for essential oils from Fructus *Alpiniae zerumbet* (EOFAZ) that targets early diabetic retinopathy stages and oxidative stress. They reported that the NPs significantly suppressed abnormal cell growth, alleviated inflammation, and reduced oxidative stress *in vitro*. The animal studies on diabetic mice showed that the synthesized NPs modulated oxidative stress and inflammation and mitigated early pathological changes. They showed that the NPSPHE@EOFA administration decreased malondialdehyde levels and increased SOD and GSH. Moreover, they found that the treatment reduced IL-6 and IL-1β levels. In another study, Zhang et al. [61] applied *Cyperus rotundus*-loaded zinc oxide NPs in diabetic retinopathy-induced rats. They assessed the effects by evaluating FBS, food intake, insulin, HbA1c, retina thickness, lipid peroxidation, CAT, GPx, SOD, HO-1, Nrf2, IL-1β, IL-18, and apoptosis-associated speck-like protein (ASC). They reported that the NPs elevated the food intake, HbA1c, fasting blood glucose, and lipid peroxidation levels and reduced CAT, SOD, insulin, and GPx level. They observed the upregulation of IL-18 and ASC and the downregulation of HO-1 and Nrf2 in diabetic rats. They concluded that the observed retinoprotective effects can be due to the potent antioxidant activities of the green synthesized zinc oxide NPs.

4 Conclusion

Oxidative stress has been identified as a significant contributing factor in the development of retinal degeneration and subsequent vision loss [62,63]. Hence, compounds possessing antioxidant characteristics significantly mitigate the detrimental impacts exerted on the neurological system by ROS and free radicals. The accumulation of these species might lead to neuronal demise. In the biomedical domain, there is a growing recognition of the significant potential of nanotechnology due to its ability to use the unique physical features of nanoscale materials [64]. In a previous study conducted by Fiorani et al. [65], it was demonstrated that non-stoichiometric nanoceria particles possess antioxidant properties and can be utilized to alleviate retinal neurodegenerative processes. This was observed in a model of intense light-induced retinal damage, where oxidative stress plays a critical role in the death of photoreceptor cells. In light of the aforementioned findings, this experimental investigation was conducted to assess the neuroprotective effectiveness of R-CeO_2NPs in a manner that closely emulates the conditions experienced by patients afflicted with retinal degeneration. In this study, the synthesis of R-CeO_2NPs was accomplished using rutin via a straightforward green chemistry method. The findings derived from using UV–visible, XRD, TEM, DLS, and Zetasizer techniques provided evidence of the

nanoscale characteristics of the biosynthesized NPs. The results showed that rutin successfully mediated the synthesis of CeO_2NPs, and the NPs have a spherical morphology with nanometric scale, good crystallinity, high zeta potential, and decorated with rutin-related surface functional groups. The *in vitro* biological evaluations showed that CeO_2NPs were cytocompatible, did not induce significant toxicity, and exhibited potent antioxidant activities. The animal studies showed that the treatment using CeO_2NPs modulated the daily food ingestion, increased the serum insulin level, and decreased the HbA1c level. Moreover, animal studies showed that treatment using R-CeO_2NPs improved the expression of Nrf2 and HO-1 mRNA and alleviated the oxidative stress of the tissue. Specifically, we sought to determine whether nanoceria retains its neuroprotective properties when administered after the onset of retinal degeneration. Consequently, the examination of retinal morphology revealed significant neuroprotection in the peripheral region of the retina, as evidenced by the preservation of the outer nuclear layer length and thickness. This finding is particularly noteworthy considering that the central region of the retina had already incurred damage prior to the initiation of the treatment.

Funding information: This work was supported by Project of Shaanxi Provincial Administration of Traditional Chinese Medicine (No. SZY-KJCYC-2023-097).

Author contributions: Hualei Chang, Zhongqiao Zhu, and Yali Ding performed experiments and collected data; all authors discussed the results and strategy; Juan Zhu supervised, directed, and managed the study. All authors approved of the version to be published.

Conflict of interest: Authors state no conflict of interest.

Ethical approval: The studies conducted on animals in our research organization(s) were approved by the Zhinanzhen Biology Ethics Committee, No.: A2025000119.

Data availability statement: The datasets generated during and/or analyzed during the current study are available from the corresponding author on reasonable request.

References

[1] Chang G, Tian S, Luo X, Xiang Y, Cai C, Zhu R, et al. Hypoglycemic effects and mechanisms of polyphenols from *Myrica rubra* pomace in type 2 diabetes (db/db) mice. Mol Nutr Food Res. 2025;69(10):e202400523.

[2] Zhang N, Wang Y, Li W, Wang Y, Zhang H, Xu D, et al. Association between serum vitamin D level and cardiovascular disease in Chinese patients with type 2 diabetes mellitus: a cross-sectional study. Sci Rep. 2025;15(1):6454.

[3] Liang J, He Y, Huang C, Ji F, Zhou X, Yin Y. The regulation of selenoproteins in diabetes: a new way to treat diabetes. Curr Pharm Des. 2024;30(20):1541–7.

[4] Fong DS, Aiello L, Gardner TW, King GL, Blankenship G, Cavallerano JD, et al. Diabetic retinopathy. Diabetes Care. 2003;26(suppl_1):s99–102.

[5] Robinson Jr WG, Tillis TN, Laver N, Kinoshita JH. Diabetes-related histopathologies of the rat retina prevented with an aldose reductase inhibitor. Exp Eye Res. 1990;50(4):355–66.

[6] Xu G, Yao Q, Weng Q, Su B, Zhang X, Xiong J. Study of urinary 8-hydroxydeoxyguanosine as a biomarker of oxidative DNA damage in diabetic nephropathy patients. J Pharm Biomed Anal. 2004;36(1):101–4.

[7] Baynes JW, Thorpe SR. Role of oxidative stress in diabetic complications: a new perspective on an old paradigm. Diabetes. 1999;48(1):1–9.

[8] Kowluru RA, Tang J, Kern TS. Abnormalities of retinal metabolism in diabetes and experimental galactosemia: VII. Effect of long-term administration of antioxidants on the development of retinopathy. Diabetes. 2001;50(8):1938–42.

[9] Du Y, Miller CM, Kern T. Hyperglycemia increases mitochondrial superoxide in retina and retinal cells. Free Radic Biol Med. 2003;35(11):1491–9.

[10] Kowluru RA, Atasi L, Ho Y-S. Role of mitochondrial superoxide dismutase in the development of diabetic retinopathy. Investig Ophthalmol Vis Sci. 2006;47(4):1594–9.

[11] Brownlee M. Biochemistry and molecular cell biology of diabetic complications. Nature. 2001;414(6865):813–20.

[12] Tang J, Kern TS. Inflammation in diabetic retinopathy. Prog Retinal Eye Res. 2011;30(5):343–58.

[13] Gloire G, Legrand-Poels S, Piette J. NF-κB activation by reactive oxygen species: fifteen years later. Biochem Pharmacol. 2006;72(11):1493–505.

[14] Kim J-A, Lau EK, Pan L, De Blanco EJC. NF-κB inhibitors from *Brucea javanica* exhibiting intracellular effects on reactive oxygen species. Anticancer Res. 2010;30(9):3295–300.

[15] Pan H-Z, Zhang H, Chang D, Li H, Sui H. The change of oxidative stress products in diabetes mellitus and diabetic retinopathy. Br J Ophthalmol. 2008;92(4):548–51.

[16] Madsen-Bouterse SA, Kowluru RA. Oxidative stress and diabetic retinopathy: pathophysiological mechanisms and treatment perspectives. Rev Endocr Metab Disord. 2008;9:315–27.

[17] Cheng X, Huang J, Li H, Zhao D, Liu Z, Zhu L, et al. Quercetin: a promising therapy for diabetic encephalopathy through inhibition of hippocampal ferroptosis. Phytomedicine. 2024;126:154887.

[18] Li W, Liu X, Liu Z, Xing Q, Liu R, Wu Q, et al. The signaling pathways of selected traditional Chinese medicine prescriptions and their metabolites in the treatment of diabetic cardiomyopathy: a review. Front Pharmacol. 2024;15:1416403.

[19] Geronikaki AA, Gavalas AM. Antioxidants and inflammatory disease: synthetic and natural antioxidants with anti-inflammatory activity. Comb Chem High Throughput Screen. 2006;9(6):425–42.

[20] Li W, Khor TO, Xu C, Shen G, Jeong W-S, Yu S, et al. Activation of Nrf2-antioxidant signaling attenuates NFκB-inflammatory response and elicits apoptosis. Biochem Pharmacol. 2008;76(11):1485–9.

[21] Bloomgarden ZT. Antioxidants and diabetes. Diabetes Care. 1997;20(4):670.
[22] Yeh P-T, Huang H-W, Yang C-M, Yang W-S, Yang C-H. Astaxanthin inhibits expression of retinal oxidative stress and inflammatory mediators in streptozotocin-induced diabetic rats. PLoS One. 2016;11(1):e0146438.
[23] Wang K, Yin J, Chen J, Ma J, Si H, Xia D. Inhibition of inflammation by berberine: Molecular mechanism and network pharmacology analysis. Phytomedicine. 2024;128:155258.
[24] Bansal AK, Bilaspuri G. Impacts of oxidative stress and antioxidants on semen functions. Vet Med Int. 2011;2011:579–86.
[25] Pingitore A, Lima GPP, Mastorci F, Quinones A, Iervasi G, Vassalle C. Exercise and oxidative stress: potential effects of antioxidant dietary strategies in sports. Nutrition. 2015;31(7–8):916–22.
[26] Celardo I, Traversa E, Ghibelli L. Cerium oxide nanoparticles: a promise for applications in therapy. J Exp Ther Oncol. 2011;9(1):47–51.
[27] Casals G, Perramón M, Casals E, Portolés I, Fernández-Varo G, Morales-Ruiz M, et al. Cerium oxide nanoparticles: a new therapeutic tool in liver diseases. Antioxidants. 2021;10(5):660.
[28] Jakupec M, Unfried P, Keppler B. Pharmacological properties of cerium compunds. Rev Physiol Biochem Pharmacol. 2005;153:101–11.
[29] Sathiyaseelan A, Saravanakumar K, Wang M-H. Cerium oxide decorated 5-fluorouracil loaded chitosan nanoparticles for treatment of hepatocellular carcinoma. Int J Biol Macromol. 2022;216:52–64.
[30] Sabouri Z, Sabouri M, Amiri MS, Khatami M, Darroudi M. Plant-based synthesis of cerium oxide nanoparticles using *Rheum turkestanicum* extract and evaluation of their cytotoxicity and photocatalytic properties. Mater Technol. 2022;37(8):555–68.
[31] Kubavat K, Trivedi P, Ansari H, Kongor A, Panchal M, Jain V, et al. Green synthesis of silver nanoparticles using dietary antioxidant rutin and its biological contour. Beni-Suef Univ J Basic Appl Sci. 2022;11(1):115.
[32] Kermani G, Karimi E, Tabrizi MH. Hybrid nanoarchitectonics of chitosan-cerium oxide nanoparticles for anticancer potentials. J Inorg Organomet Polym Mater. 2022;32(7):2591–9.
[33] Yiling W, Murakonda GK, Jarubula R. Application of green-synthesized cerium oxide nanoparticles to treat spinal cord injury and cytotoxicity evaluation on paediatric leukaemia cells. Mater Res Express. 2021;8(7):075006.
[34] Khorrami S, Zarepour A, Zarrabi A. Green synthesis of silver nanoparticles at low temperature in a fast pace with unique DPPH radical scavenging and selective cytotoxicity against MCF-7 and BT-20 tumor cell lines. Biotechnol Rep. 2019;24:e00393.
[35] Baliyan S, Mukherjee R, Priyadarshini A, Vibhuti A, Gupta A, Pandey RP, et al. Determination of antioxidants by DPPH radical scavenging activity and quantitative phytochemical analysis of *Ficus religiosa*. Molecules. 2022;27(4):1326.
[36] Yakoob AT, Tajuddin NB, Hussain MIM, Mathew S, Govindaraju A, Qadri I. Antioxidant and hypoglycemic activities of *Clausena anisata* (Willd.) Hook F. ex benth. root mediated synthesized silver nanoparticles. Pharmacogn J. 2016;8(6):686137.
[37] Ghasemi A, Jeddi S. Streptozotocin as a tool for induction of rat models of diabetes: a practical guide. EXCLI J. 2023;22:274.
[38] Ansari AA, Labis JP, Alam M, Ramay SM, Ahmad N, Mahmood A. Synthesis, structural and optical properties of Mn-doped ceria nanoparticles: a promising catalytic material. Acta Metall Sin (Engl Lett). 2016;29:265–73.
[39] Maqbool Q, Nazar M, Naz S, Hussain T, Jabeen N, Kausar R, et al. Antimicrobial potential of green synthesized CeO_2 nanoparticles from *Olea europaea* leaf extract. Int J Nanomed. 2016;11:5015–25.
[40] Li S, Hu S, Jiang W, Liu Y, Zhou Y, Liu J, et al. Facile synthesis of cerium oxide nanoparticles decorated flower-like bismuth molybdate for enhanced photocatalytic activity toward organic pollutant degradation. J Colloid Interface Sci. 2018;530:171–8.
[41] Badirzadeh A, Alipour M, Najm M, Vosoogh A, Vosoogh M, Samadian H, et al. Potential therapeutic effects of curcumin coated silver nanoparticle in the treatment of cutaneous leishmaniasis due to Leishmania major in-vitro and in a murine model. J Drug Delivery Sci Technol. 2022;74:103576.
[42] Bhattacharjee S. DLS and zeta potential – what they are and what they are not? J Controlled Rel. 2016;235:337–51.
[43] Habib IY, Kumara N, Lim CM, Mahadi AH. Dynamic light scattering and zeta potential studies of ceria nanoparticles. Solid State Phenom. 2018;278:112–20.
[44] Ornatska M, Sharpe E, Andreescu D, Andreescu S. Paper bioassay based on ceria nanoparticles as colorimetric probes. Anal Chem. 2011;83(11):4273–80.
[45] Koosha F, Farsangi ZJ, Samadian H, Amini SM. Mesoporous silica coated gold nanorods: a multifunctional theranostic platform for radiotherapy and X-ray imaging. J Porous Mater. 2021;28(6):1961–8.
[46] Clogston JD, Patri AK. Zeta potential measurement. Characterization of nanoparticles intended for drug delivery. Springer; 2011. p. 63–70
[47] Salopek B, Krasic D, Filipovic S. Measurement and application of zeta-potential. Rudarsko-geolosko-naftni zbornik. 1992;4(1):147.
[48] Gulicovski JJ, Bračko I, Milonjić SK. Morphology and the isoelectric point of nanosized aqueous ceria sols. Mater Chem Phys. 2014;148(3):868–73.
[49] Taherzadeh D, Amiri H, Ebrahimi S, Ghafarpour A, Samandarinejad N, Darroudi M, et al. Green synthesis of cerium oxide nanoparticles using *Falcaria vulgaris* leaf extract and its anti-tumoral effects in prostate cancer. Methods in Molecular Biology (MIMB), vol. 697, 2023, p. 63–70.
[50] Hancock ML, Yokel RA, Beck MJ, Calahan JL, Jarrells TW, Munson EJ, et al. The characterization of purified citrate-coated cerium oxide nanoparticles prepared via hydrothermal synthesis. Appl Surf Sci. 2021;535:147681.
[51] Finkel T. Oxidant signals and oxidative stress. Curr OpCell Biol. 2003;15(2):247–54.
[52] Dröge W. Free radicals in the physiological control of cell function. Physiol Rev. 2002;82(1):47–95.
[53] Evans JL, Goldfine ID, Maddux BA, Grodsky GM. Are oxidative stress-activated signaling pathways mediators of insulin resistance and β-cell dysfunction? Diabetes. 2003;52(1):1–8.
[54] Keser S, Celik S, Turkoglu S, Yilmaz O, Turkoglu I. Hydrogen peroxide radical scavenging and total antioxidant activity of hawthorn. Chem J. 2012;2(1):9–12.
[55] Mansouri A, Makris DP, Kefalas P. Determination of hydrogen peroxide scavenging activity of cinnamic and benzoic acids employing a highly sensitive peroxyoxalate chemiluminescence-based assay: structure–activity relationships. J Pharm Biomed Anal. 2005;39(1–2):22–6.
[56] Lopez-Pascual A, Urrutia-Sarratea A, Lorente-Cebrián S, Martinez JA, González-Muniesa P. Cerium oxide nanoparticles regulate insulin sensitivity and oxidative markers in 3T3-L1 adipocytes and C2C12 myotubes. Oxid Med Cell Longev. 2019;2019(1):2695289.

[57] Khan M, Sohail A, Raja NI, Asad MJ, Mashwani Z-u-R. Antioxidant and hypoglycemic potential of phytogenic cerium oxide nanoparticles. Sci Rep. 2023;13(1):4514.
[58] Calderon G, Juarez O, Hernandez G, Punzo S, De la Cruz Z. Oxidative stress and diabetic retinopathy: development and treatment. Eye. 2017;31(8):1122–30.
[59] Haydinger CD, Oliver GF, Ashander LM, Smith JR. Oxidative stress and its regulation in diabetic retinopathy. Antioxidants. 2023;12(8):1649.
[60] Li J, Liu Y, Geng K, Lu X, Shen X, Guo Q. ROS-responsive nanoparticles with antioxidative effect for the treatment of diabetic retinopathy. J Biomater Sci Polym Ed. 2025;36(4):440–61.
[61] Zhang L, Chu W, Zheng L, Li J, Ren Y, Xue L, et al. Zinc oxide nanoparticles from *Cyperus rotundus* attenuates diabetic retinopathy by inhibiting NLRP3 inflammasome activation in STZ-induced diabetic rats. J Biochem Mol Toxicol. 2020;34(12):e22583.
[62] Swaroop A, Chew EY, Bowes Rickman C, Abecasis GR. Unraveling a multifactorial late-onset disease: from genetic susceptibility to disease mechanisms for age-related macular degeneration. Annu Rev Genomics Hum Genet. 2009;10:19–43.
[63] Ting AY, Lee TK, MacDonald IM. Genetics of age-related macular degeneration. Curr Opin Ophthalmol. 2009;20(5):369–76.
[64] Kim E-M, Jeong H-J. Current status and future direction of nanomedicine: focus on advanced biological and medical applications. Nucl Med Mol Imaging. 2017;51:106–17.
[65] Fiorani L, Passacantando M, Santucci S, Di Marco S, Bisti S, Maccarone R. Cerium oxide nanoparticles reduce microglial activation and neurodegenerative events in light damaged retina. PLoS One. 2015;10(10):e0140387.